Tailoring Multiloop Atom Interferometers with Adjustable Momentum Transfer

L. A. Sidorenkov[*], R. Gautier, M. Altorio, R. Geiger,[†] and A. Landragin

LNE-SYRTE, Observatoire de Paris-Université PSL,
CNRS, Sorbonne Université, 61 avenue de l'Observatoire, 75014 Paris, France

Multiloop matter-wave interferometers are essential in quantum sensing to measure the derivatives of physical quantities in time or space. Because multiloop interferometers require multiple reflections, imperfections of the matter-wave mirrors create spurious paths that scramble the signal of interest. Here, we demonstrate a method of adjustable momentum transfer that prevents the recombination of the spurious paths in a double-loop atom interferometer aimed at measuring rotation rates. We experimentally study the recombination condition of the spurious matter waves, which is quantitatively supported by a model accounting for the coherence properties of the atomic source. We finally demonstrate the effectiveness of the method in building a cold-atom gyroscope with a single-shot acceleration sensitivity suppressed by a factor of at least 50. Our study will impact the design of multiloop atom interferometers that measure a single inertial quantity.

Matter-wave interference is a central concept of quantum mechanics with a myriad of applications making use of electrons [1], neutrons [2], or atoms and molecules [3]. Examples of applications range from bacteria characterization [4] and biomolecular analysis [5], to fundamental physics tests [6] and accurate inertial sensing [7]. In most cases, the signal of interest can be detected as it shifts the phase of a sinusoidal interference fringe pattern of two partial waves. However, the presence of auxiliary interferometric loops due to the imperfection of the mirrors results in a multiple-wave interference, which reduces the interference contrast and the phase measurement accuracy.

Light-pulse atom interferometers employ a train of laser pulses that split, deflect, and recombine the atomic waves to enclose a single loop Mach-Zehnder interferometer, in the simplest case. Here, the light pulses act as atom optical beam splitters and mirrors, respectively. Oftentimes, one may be interested in field derivatives rather than the fields themselves (e.g., gradients of the gravitational field or curvature of a magnetic field), or in a selective measurement in a given frequency band. This is realized with interferometers consisting of several loops [8,9], realized by multiple deflection of the matter waves with additional mirrors—a technique analogous to the multipulse magnetic resonance spectroscopy [10].

The atom optics relies on coherent atom-light interaction, whose efficiency is limited by the homogeneity of the effective Rabi coupling that depends on the local laser intensity and velocity of the atom. The challenge arises when the nonzero transmission of the atomic mirrors leads to leakage of the matter waves, which are redirected by subsequent mirrors and eventually form undesired additional interferometer loops, thus degrading the two-wave

nature of the interferometer [11]. Understanding and controlling the recombination of these spurious paths is intimately linked to the coherence of the matter-wave source, and requires a tailored design of the interferometric sequence and atomic mirrors.

In this Letter, we report on a method which prevents the recombination of spurious paths in multiloop cold-atom interferometers using mirrors that transfer an adjustable momentum to the atom. The high degree of control of this method, compared to other techniques in matter-wave interferometry, enables a detailed study of the recombination of wave packets. We show that the method of adjustable momentum transfer (AMT) allows for building a pure-rate gyroscope (i.e., fully sensitive to rotation rate and insensitive to acceleration), as proposed in Ref. [12]. Our result can be generalized to atom-interferometer sensors of arbitrary multiloop architectures.

We implement the AMT method in a double-loop atom interferometer aimed at measuring rotation rates and described in Refs. [13,14]. In short, we laser cool cesium atoms in a single internal state $|F = 4\rangle$ to the temperature of 1.8 μK, and launch them vertically using moving molasses in an atomic fountain. The atom optics employ stimulated Raman transitions at 852 nm that couple the $|F = 3\rangle$ and $|F = 4\rangle$ internal states with two counter-propagating laser fields of wave vectors $\vec{k}_3$ and $\vec{k}_4$, imparting a momentum $\hbar\vec{k}_{\text{eff}} = \hbar(\vec{k}_3 - \vec{k}_4)$ to the diffracted part of the wave packet [15]. The interferometric sequence comprising four Raman laser pulses of $\pi/2, \pi, \pi, \pi/2$ Rabi angles, forms a symmetric double-loop interferometer. Since the momentum of the atoms is entangled with their internal state, the accumulated atomic phase difference is read out from the final population difference of the
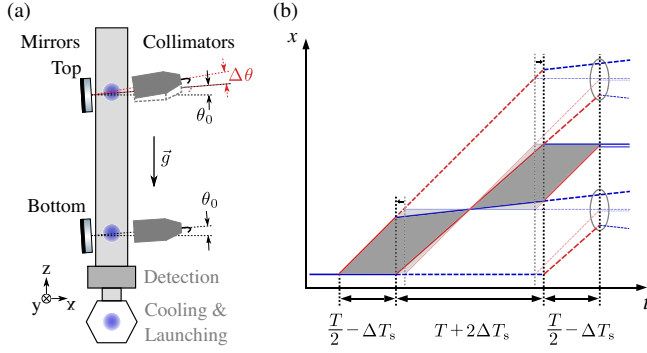
FIG. 1.   (a) Schematics of the cold-atom gyroscope sensor. The angular tilt $\Delta\theta$ of the top collimator allows for adjusting the effective momentum transfer of the π pulses. (b) Space-time diagram (not to scale) of the time-symmetric four-pulse interferometric sequence in the original equal-k_{eff} (thin half-transparent lines) and AMT (thick full lines) cases. Red (blue) color labels $F = 3$ ($F = 4$) internal state of the atoms. Solid (dashed) trajectories correspond to the main (spurious) interferometers. For equal-k_{eff} (AMT) sequence: the vertical dashed gray (black) lines indicate the timings of the pulses; light- (dark-) gray areas highlight the two loops of the main interferometer. Gray ovals mark the spatial separation of the spurious wave packets at the last pulse in the AMT sequence. For clarity, we show only the output ports labeled by the $F = 4$ state.

two hyperfine states, as determined by fluorescence detection [16].

Two pairs of retroreflected Raman beams interact with the atomic cloud at different height as shown in Fig. 1(a). The two mirrors are parallel to each other to better than 0.4 μrad (see Ref. [17] for the alignment procedure). The normal to the mirrors, which sets the direction of the effective wave vector $\vec{k}_{\mathrm{eff}}$, is inclined by an angle $\theta_0 = 3.8°$ with respect to the horizontal direction $\hat{x}$ (perpendicular to gravity), in order to lift the degeneracy between the $\pm\hbar k_{\mathrm{eff}}$ transitions owing to the Doppler effect. The top collimator can be further inclined by a small adjustable angle $\Delta\theta \lesssim 20$ mrad, leading to a reduced modulus of the effective Raman wave vector of the top beam $k_{\mathrm{eff}}^{(T)}$ with respect to the bottom one, $k_{\mathrm{eff}}^{(B)} \equiv k_{\mathrm{eff}}$, without changing its direction:

$$k_{\mathrm{eff}}^{(B)} - k_{\mathrm{eff}}^{(T)} = \epsilon k_{\mathrm{eff}} \approx \frac{\Delta\theta^2}{2} k_{\mathrm{eff}}. \qquad (1)$$

This scheme, where the two wave vectors are not equal (as theoretically studied in Ref. [18] in the context of recoil frequency measurements) allows us to reach the necessary change in the momentum transfer to prevent the recombination of spurious paths in multiloop interferometers with cold-atom sources. Adjusting the momentum transfer could also be realized by shifting the frequencies of the lasers, as proposed in Ref. [19] and implemented in Refs. [20–22] to reduce systematic errors in single-loop gravity sensors.

However, this would require frequency changes of tens of gigahertz, which makes it impractical, here.

In the traditional double-loop sequence [11,13] [Fig. 1(b), thin half-transparent lines], the four Raman laser pulses are separated by time intervals $T/2$, T, and $T/2$, with $T = 400$ ms. The time symmetry of this sequence with respect to the apogee of the atomic trajectory (crossing of the two loops at $t = t_1 + T$, t_1 being the timing of the first pulse with respect to the launch) leads to a vanishing sensitivity to constant linear acceleration, which is required to build a pure-rate gyroscope. However, two spurious Ramsey-Bordé-like [23] interferometers [thin dashed lines in Fig. 1(b)] recombine simultaneously with the main one and, having different inertial sensitivity, impair the signal of interest. Distinguishing the spurious interferometers from the main one would require a position-sensitive detector (along the $\hat{x}$ direction) and an atomic source with subrecoil temperature, which would add complexity to the sensor architecture.

To circumvent this problem, one may apply a small asymmetric time shift of the mirror pulses (both pulses delayed or advanced by ΔT_a) [11], inducing sufficient spatial separation of the spurious wave packets while barely modifying the rotation-rate sensitivity of the main interferometer. Braking its time symmetry, nonetheless, imbalances the space-time areas of the two loops, which causes a sensitivity to constant linear acceleration.

The thick solid trajectory lines in Fig. 1(b) show the interferometer sequence using AMT as explored in this Letter. In order to close the main interferometer, the reduction of the momentum transfer at the π pulses governed by Eq. (1) is compensated with their shift in time [see Fig. 1(b)] of

$$\Delta T_s = \frac{T\epsilon}{2(1 - \epsilon)}. \qquad (2)$$

The new degree of freedom provided by AMT allows us to retain the original time symmetry of the main interferometer and to prevent the recombination of the spurious wave packets, on which we will focus in the following.

In order to sufficiently separate the recombination time of the spurious interferometers from that of the main one (see Supplemental Material, Sec. S3 [24]), we shift the mirror pulses by a fixed time interval $\Delta T = 40$ μs as shown in Fig. 2(a). We also deliberately enhance the amplitudes in the spurious branches by changing the Rabi angles of these pulses from π to $\pi/2$, thus making the mirrors half-transparent. Finally, we introduce a controlled variable delay of the third pulse, ΔT_3 [see Fig. 2(a)], that allows us to probe the efficiency of the recombination of the spurious interferometers.

In Fig. 2(b) we present the evolution of the contrast of the spurious interferometers as we gradually transform the sequence with increasing value of the angle $\Delta\theta$. For each
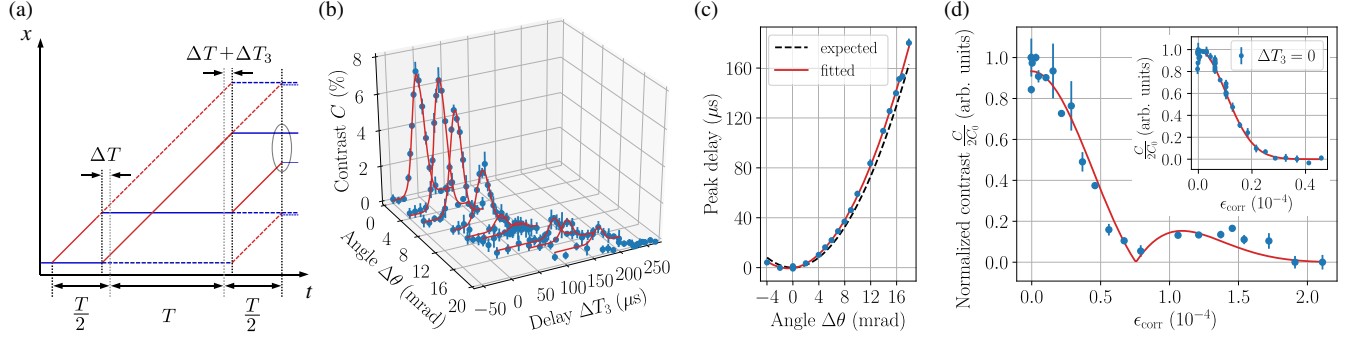
FIG. 2.   (a) Space-time diagram of the interferometer to introduce the definitions of the fixed $\Delta T = 40$ μs and the variable ΔT_3. (b) Peak-peak contrast of the spurious interferometers (blue dots) as a function of the third pulse delay ΔT_3, for a set of angles $\Delta\theta$, and Gaussian fits (solid red lines) to the corresponding data. (c) Fitted values of ΔT_3 yielding maximum contrast for the probed values of $\Delta\theta$. Dashed black line is the expectation of $\Delta T_3 = 2\epsilon(T + t_1)$, solid red line is the fit to the data accounting for initial angular offsets $\Delta\theta_{0z}$, $\Delta\theta_{0y}$. (d) Normalized fitted peak contrast for the probed values of $\epsilon_{\mathrm{corr}} = \frac{1}{2}[(\Delta\theta - \Delta\theta_{0z})^2 - \Delta\theta_{0y}^2]$. The solid red line is the fit with Eq. (5) with σ_r and C_0 as free parameters (see text). Inset: contrast decay for $\Delta T_3 = 0$. The solid red line is the expectation for the measured value of σ_v and the fitted value of σ_r.

angle, we probe the spurious signal by scanning the value of ΔT_3 (blue dots). At $\Delta\theta = 0$, we find the maximum of the contrast, as expected, around $\Delta T_3 = 0$ μs. We observe a reduction of the maximum contrast while increasing $\Delta\theta$ toward an almost full suppression around $\Delta\theta = 12$ mrad, followed by a clear revival and a final decay at large angles. To connect the observed contrast behavior with the coherence properties of the cold-atom source, we derive the phase shifts of the bottom (B) and top (T) spurious interferometers (see Supplemental Material, Sec. S1 [24]) as

$$\Delta\Phi^{(B)} = \Delta\Phi_r(r_0) + \Delta\Phi_v(v_0) + \Delta\Phi' - \omega_R T\epsilon,$$
$$\Delta\Phi^{(T)} = \Delta\Phi_r(r_0) + \Delta\Phi_v(v_0) + \Delta\Phi' + \omega_R T\epsilon, \quad (3)$$

where $\omega_R \equiv \hbar k_{\mathrm{eff}}^2/2m$ is the two-photon recoil frequency and

$$\Delta\Phi_r(r_0) = 2\vec{k}_{\mathrm{eff}} \cdot \vec{r}_0\epsilon$$
$$\Delta\Phi_v(v_0) = \vec{k}_{\mathrm{eff}} \cdot \vec{v}_0[2\epsilon(T + t_1) - \Delta T_3]. \quad (4)$$

We express the phase shifts as a sum of four distinct terms. The first two terms, $\Delta\Phi_r(r_0)$ and $\Delta\Phi_v(v_0)$, depend on the initial (at launch) position $\vec{r}_0 = \vec{r}(t = 0)$ and velocity $\vec{v}_0 = \vec{v}(t = 0)$ of a given atom in the reference frame of the center of mass of the atomic cloud. The third term $\Delta\Phi'$ incorporates the inertial contribution due to acceleration and the common recoil phase shift. The last term constitutes a relative dephasing of the two spurious interferometers, which increases with ϵ.

The contrast of the spurious interferometric signal $C(\epsilon, \Delta T_3)$ is given by the (incoherent) sum of the intensities from both interferometers, averaged over the initial statistical velocity and position distributions of the atomic source. We assume uncorrelated Gaussian velocity

and position distributions, respectively characterized by the standard deviations σ_v and σ_r, and obtain (see Supplemental Material, Sec. S2 [24]):

$$\frac{C(\epsilon, \Delta T_3)}{2C_0} = |\cos(\omega_R T\epsilon)|e^{-(1/2)[\Delta\Phi_r(\sigma_r)^2 + \Delta\Phi_v(\sigma_v)^2]}, \quad (5)$$

where C_0 is the maximum mean contrast. The oscillating term reflects the recoil-originated dephasing between the two spurious interferometers, while the exponential suppression factor highlights the role of the finite spatial and momentum spread in the cold-atom source.

The effect of the finite velocity spread on the contrast can be fully eliminated by the proper choice of $\Delta T_3 = 2\epsilon(T + t_1)$ [from Eq. (4)], which defines the recombination in momentum space and therefore yields the maximum of contrast. This expectation for ΔT_3, shown by the dashed black line in Fig. 2(c), qualitatively matches the data (blue dots). A quantitative agreement is obtained by accounting for the initial angular mismatch between the collimators in both z (vertical) and y (horizontal) directions via $\epsilon_{\mathrm{corr}} = [(\Delta\theta - \Delta\theta_{0z})^2 - \Delta\theta_{0y}^2]/2$ [30]. Fitting the data with $\Delta T_3 = 2\epsilon_{\mathrm{corr}}(T + t_1)$ [solid red line in Fig. 2(b)] reveals small angular offsets $\Delta\theta_{0z} = -0.68(5)$ mrad and $\Delta\theta_{0y} = 1.04(19)$ mrad, which are compatible with the inaccuracy of the initial manual tuning of the collimator of about 1 mrad.

In Fig. 2(d) we plot the values of fitted maximum contrast of the spurious interferometers normalized to the maximum value among all the datasets, for different values of ϵ_{corr}. The overall trend, including the zero and the revival, is well reproduced by the fit (solid red line) with the model of Eq. (5) accounting for $\Delta\Phi_v = 0$ (recombination in momentum space), with C_0 and σ_r as free parameters. The fitted value of $\sigma_r = 0.51(2)$ mm sets the realistic scale for the spatial extent of the atomic cloud. A non-Gaussian
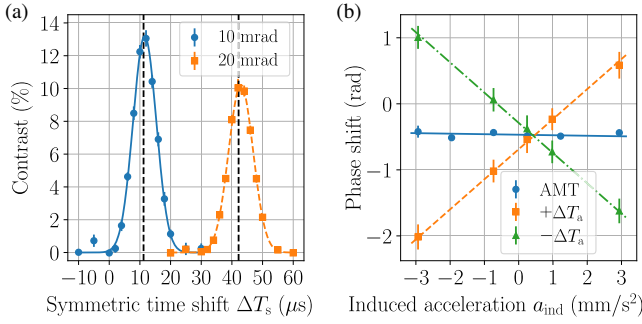
FIG. 3. (a) Contrast of the main interferometer in the AMT configuration as a function of symmetric time shift ΔT_s, for two values of the angle $\Delta\theta$. The solid blue and dashed orange lines are empiric Gaussian fits to the data. The vertical dashed lines mark the expected center positions. (b) Phase shift as a function of induced acceleration (see text), in the AMT case with $\Delta\theta = 20$ mrad and $\Delta T_s = 42.9$ μs (blue dots), and in the asymmetric case with $\Delta T_a = \pm 40$ μs (orange squares and green triangles). Solid blue, dashed orange, and dash-dotted green lines are linear fits to the data.

actual cloud shape might be the cause of the slight mismatch around $\epsilon_{corr} \simeq 1.6 \times 10^{-4}$.

The inset of Fig. 2(d) shows the contrast decay in the case of $\Delta T_3 = 0$ (where $\Delta\Phi_v \neq 0$), which is driven by the finite velocity spread of the source and happens on a much faster ϵ scale. This behavior does not depend on the specific value of $\Delta T = 40$ μs, and is thus also applicable to the case of $\Delta T = \Delta T_s$ [Fig. 1(b)]. The complete suppression of the signal of the spurious loops in the time-symmetric AMT sequence therefore happens on a scale of $\epsilon \simeq 4 \times 10^{-5}$. These data are well matched by the expected behavior of Eq. (5) (solid red line), with the value of σ_v extracted from the widths of the peaks in the panel (b) (see Supplemental Material, Sec. S3 [24]).

We now focus on the main (double-loop) interferometer in the time-symmetric AMT configuration of Fig. 1(b). The promised insensitivity to the dc acceleration of this sequence, in practice, relies on the ability to accurately meet the condition of Eq. (2). In Fig. 3(a), we probe the recombination of the main interferometer for the applied values of $\Delta\theta = 10$ mrad and 20 mrad by scanning the time shift ΔT_s and recording the peak-peak contrast. We find the peak centers at 11.6(1) μs and 42.9(1) μs, very close to their respective expectation of Eq. (2) with $\epsilon = \epsilon_{corr}$ at 11.2 μs and 42.2 μs.

We choose the AMT arrangement with $\Delta\theta = 20$ mrad and $\Delta T_s = 42.9$ μs to verify the insensitivity of the main interferometer to the linear dc acceleration. We induce an additional acceleration along the k_{eff} direction via controlled tilt of the sensor in x–z plane by a small angle β such that $a_{ind} = g\cos\theta_0\sin\beta$, and measure the corresponding phase shift [blue dots in Fig. 3(b)]. The fitted residual linear slope $d\Phi/da_{ind} = 0.4(8.5)$ rad/(m s^{-2}) [blue line in Fig. 3(b)] is compatible with zero within the error bar.

For comparison, we perform an identical measurement in the asymmetric configuration [11,13] where both mirror pulses are advanced ($\Delta T_a = 40$ μs, orange squares) or delayed ($\Delta T_a = -40$ μs, green triangles). For this configuration, we extract the respective dc-acceleration-sensitivity slopes of $446(8)$ rad/(m s^{-2}) and $-448(5)$ rad/(m s^{-2}) matching within 5% the expectation of $d\Phi/da_{ind} = 2T\Delta T_a k_{eff}$. The ratio of the modulus of the slopes reflects a suppression of the acceleration-induced phase shift in a single measurement using the symmetric AMT configuration, as compared to the asymmetric one, by at least the factor of 50.

We finally consider the impact of the AMT technique on the phase shift of the gyroscope sensor, which is given by (see Supplemental Material, Sec. S4 [24])

$$\Delta\Phi = \frac{1}{2}\vec{k}_{eff}(\vec{g} \times \vec{\Omega})T^3\left(1 - \frac{2\epsilon}{3}\right) + \Delta\omega_0\frac{2T\epsilon}{(1-\epsilon)}. \quad (6)$$

The first term accounts for a correction to the gyroscope scale factor, as can be derived from the reduction of the physical (Sagnac) area of the interferometer, with $\vec{\Omega}$ being the rotation rate of the Earth. The second term (called hereafter clock shift) represents the sensitivity to the detuning ($\Delta\omega_0$) of the relative Raman laser frequencies from the resonance condition of the Raman transition at the apogee point.

We measured the clock shift and confirmed the expected behavior of Eq. (6) (see Supplemental Material, Sec. S4 [24]). By alternating measurements with $\pm k_{eff}$, we could demonstrate a rejection of this clock shift by at least 2 orders of magnitude, yielding a residual sensitivity for $\Delta\theta = 20$ mrad compatible with zero and below 10 mrad/kHz. The study of the correction to the gyroscope scale factor [first term of Eq. (6)] goes beyond the scope of this Letter.

To conclude, we have demonstrated the method of adjustable momentum transfer in multiloop atom interferometers, that provides a controlled suppression of the spurious interferometric signals originating from the finite efficiency of atomic mirrors. The observed variation of the contrast of the spurious interferometers, quantitatively supported by our model, revealed a fractional imbalance in momentum transfer of $\epsilon \simeq 4 \times 10^{-5}$ to completely suppress the spurious signals, as given by the finite coherence of our atom source. In addition, we discovered a remarkable configuration ($\omega_R T\epsilon = \pi/2$), where the spurious interferometers are in antiphase due to their different recoil sensitivity. The AMT method allowed us to demonstrate a double-loop gyroscope with a highly suppressed sensitivity to constant linear acceleration. This holds particular interest for applications where the fluctuations of the rotation rate of the ground need to be discriminated from the linear translations, as for example, in the field of rotational seismology [31].

Our results pave the way for the design of sensors with atomic sources of increased coherence or with more than two interferometric loops, where the problems associated with spurious paths are enhanced. More generally, our work shows the possibility of tuning the sensitivity of multiloop atom interferometers to a unique, chosen, physical quantity, which enables to extend the scope of atom interferometry to new domains. This is crucial for multiloop atom interferometers used as gravity gradiometers [9,32] and gyroscopes [11,13,33], or proposed for gravitational wave detection [34–37] or for measuring spacetime curvature [38].

*leonid.sidorenkov@gmail.com
†remi.geiger@obspm.fr

[1] G. F. Missiroli, G. Pozzi, and U. Valdre, Electron interferometry and interference electron microscopy, J. Phys. E **14,** 649 (1981).

[2] H. Rauch, S. A. Werner, and P. E. H. Rauch, *Neutron Interferometry: Lessons in Experimental Quantum Mechanics*, Oxford in Asia. Historical Reprints (Clarendon Press, Oxford, 2000).

[3] A. D. Cronin, J. Schmiedmayer, and D. E. Pritchard, Optics and interferometry with atoms and molecules, Rev. Mod. Phys. **81,** 1051 (2009).

[4] R. E. Dunin-Borkowski, M. R. McCartney, R. B. Frankel, D. A. Bazylinski, M. Pósfai, and P. R. Buseck, Magnetic microstructure of magnetotactic bacteria by electron holography, Science **282,** 1868 (1998).

[5] M. Arndt, N. Drre, S. Eibenberger, P. Haslinger, J. Rodewald, K. Hornberger, S. Nimmrichter, and M. Mayor, Matter-wave interferometry with composite quantum objects, arXiv:1501.07770.

[6] H. Abele and H. Leeb, Gravitation and quantum interference experiments with neutrons, New J. Phys. **14,** 055010 (2012).

[7] R. Geiger, A. Landragin, S. Merlet, and F. Pereira Dos Santos, High-accuracy inertial measurements with cold-atom sensors, AVS Quantum Sci. **2,** 024702 (2020).

[8] J. F. Clauser, Ultra-high sensitivity accelerometers and gyroscopes using neutral atom matter-wave interferometry, Physica (Amsterdam) **151B+C,** 262 (1988).

[9] J. M. McGuirk, G. T. Foster, J. B. Fixler, M. J. Snadden, and M. A. Kasevich, Sensitive absolute-gravity gradiometry using atom interferometry, Phys. Rev. A **65,** 033608 (2002).

[10] H. Y. Carr and E. M. Purcell, Effects of diffusion on free precession in nuclear magnetic resonance experiments, Phys. Rev. **94,** 630 (1954).

[11] J. K. Stockton, K. Takase, and M. A. Kasevich, Absolute Geodetic Rotation Measurement Using Atom Interferometry, Phys. Rev. Lett. **107,** 133001 (2011).

[12] B. Dubetsky and M. A. Kasevich, Atom interferometer as a selective sensor of rotation or gravity, Phys. Rev. A **74,** 023615 (2006).

[13] I. Dutta, D. Savoie, B. Fang, B. Venon, C. L. Garrido Alzar, R. Geiger, and A. Landragin, Continuous Cold-Atom Inertial sensor with 1 nrad/sec rotation stability, Phys. Rev. Lett. **116,** 183003 (2016).

[14] D. Savoie, M. Altorio, B. Fang, L. A. Sidorenkov, R. Geiger, and A. Landragin, Interleaved atom interferometry for high-sensitivity inertial measurements, Sci. Adv. **4,** eaau7948 (2018).

[15] M. Kasevich and S. Chu, Atomic Interferometry Using Stimulated Raman Transitions, Phys. Rev. Lett. **67,** 181 (1991).

[16] Ch. J. Bordé, Atomic interferometry with internal state labelling, Phys. Lett. A **140,** 10 (1989).

[17] M. Altorio, L. A. Sidorenkov, R. Gautier, D. Savoie, A. Landragin, and R. Geiger, Accurate trajectory alignment in cold-atom interferometers with separated laser beams, Phys. Rev. A **101,** 033606 (2020).

[18] B. Dubetsky, Asymmetric Mach-Zehnder atom interferometers, arXiv:1710.00020.

[19] A. Roura, Circumventing Heisenberg's Uncertainty Principle in Atom Interferometry Tests of the Equivalence Principle, Phys. Rev. Lett. **118,** 160401 (2017).

[20] G. D'Amico, G. Rosi, S. Zhan, L. Cacciapuoti, M. Fattori, and G. M. Tino, Canceling the Gravity Gradient Phase Shift in Atom Interferometry, Phys. Rev. Lett. **119,** 253201 (2017).

[21] C. Overstreet, P. Asenbaum, T. Kovachy, R. Notermans, J. M. Hogan, and M. A. Kasevich, Effective Inertial Frame in an Atom Interferometric Test of the Equivalence Principle, Phys. Rev. Lett. **120,** 183604 (2018).

[22] R. Caldani, K. X. Weng, S. Merlet, and F. Pereira Dos Santos, Simultaneous accurate determination of both gravity and its vertical gradient, Phys. Rev. A **99,** 033601 (2019).

[23] Ch. J. Bordé, Ch. Salomon, S. Avrillier, A. van Lerberghe, Ch. Bréant, D. Bassi, and G. Scoles, Optical Ramsey fringes with traveling waves, Phys. Rev. A **30,** 1836 (1984).

[24] See Supplemental Material at http://link.aps.org/supplemental/10.1103/PhysRevLett.125.213201 for the calculation of the phase shift of the spurious interferometers and their contrast, for additional data on the spurious interferometers, and for details of the phase shift of the main, double-loop interferometer, which includes Refs. [25–29].

[25] P. Wolf, L. Blanchet, C. J. Bordé, S. Reynaud, C. Salomon, and C. Cohen-Tannoudji, Does an atom interferometer test the gravitational redshift at the Compton frequency?, Classical Quantum Gravity **28,** 145017 (2011).

[26] P. Storey and C. Cohen-Tannoudji, The Feynman path integral approach to atomic interferometry. A tutorial. J. Phys. II (France) **4,** 1999 (1994).

[27] D. M. S. Johnson, Long baseline atom interferometry, Ph.D. Thesis, Stanford University, 2011.

[28] Ch. Antoine and Ch. J. Bordé, Quantum theory of atomic clocks and gravito-inertial sensors: An update, J. Opt. B **5,** S199 (2003).

[29] P. Cheinet, B. Canuel, F. Pereira Dos Santos, A. Gauguet, F. Yver-Leduc, and A. Landragin, Measurement of the sensitivity function in a time-domain atomic interferometer, IEEE Trans. Instrum. Meas. **57,** 1141 (2008).

[30] The minus sign in front of the $\Delta\theta_{0y}^2$ indicates that the bottom collimator is more tilted than the top one in the y (horizontal) direction.

[31] C. Hadziioannou, P. Gaebler, U. Schreiber, J. Wassermann, and H. Igel, Examining ambient noise using colocated measurements of rotational and translational motion, J. Seismol. **16,** 787 (2012).

[32] I. Perrin, Y. Bidel, N. Zahzam, C. Blanchard, A. Bresson, and M. Cadoret, Proof-of-principle demonstration of vertical-gravity-gradient measurement using a single-proof-mass double-loop atom interferometer, Phys. Rev. A **99,** 013601 (2019).

[33] B. Canuel, F. Leduc, D. Holleville, A. Gauguet, J. Fils, A. Virdis, A. Clairon, N. Dimarcq, Ch. J. Bordé, A. Landragin,

and P. Bouyer, Six-Axis Inertial Sensor Using Cold-Atom Interferometry, Phys. Rev. Lett. **97,** 010402 (2006).

[34] J. M. Hogan, D. M. S. Johnson, S. Dickerson, T. Kovachy, A. Sugarbaker, S.-w. Chiow, P. W. Graham, M. A. Kasevich, B. Saif, S. Rajendran, P. Bouyer, B. D. Seery, L. Feinberg, and R. Keski-Kuha, An atomic gravitational wave interferometric sensor in low earth orbit (agis-leo), Gen. Relativ. Gravit. **43,** 1953 (2011).

[35] P. W. Graham, J. M. Hogan, M. A. Kasevich, and S. Rajendran, Resonant mode for gravitational wave detectors based on atom interferometry, Phys. Rev. D **94,** 104022 (2016).

[36] B. Canuel *et al.*, Exploring gravity with the MIGA large scale atom interferometer, Sci. Rep. **8,** 14064 (2018).

[37] C. Schubert, D. Schlippert, S. Abend, E. Giese, A. Roura, W. P. Schleich, W. Ertmer, and E. M. Rasel, Scalable, symmetric atom interferometer for infrasound gravitational wave detection, arXiv:1909.01951.

[38] K.-P. Marzlin and J. Audretsch, State independence in atom interferometry and insensitivity to acceleration and rotation, Phys. Rev. A **53,** 312 (1996).